Earth regeneration effect in solar neutrino oscillations: An analytic approach

Eligio Lisi and Daniele Montanino

Dipartimento di Fisica and Sezione INFN di Bari, Via Amendola 173, I-70126 Bari, Italy

We present a simple and accurate method for computing analytically the regeneration probability of solar neutrinos in the Earth. We apply this method to the calculation of several solar-model-independent quantities that can be measured by the SuperKamiokande and Sudbury Neutrino Observatory experiments. [S0556-2821(97)01015-1]

I. INTRODUCTION

The Mikheyev-Smirnov-Wolfenstein (MSW) mechanism of neutrino oscillations in matter [1] represents a fascinating solution to the long-standing solar neutrino problem [2]. The possible observation of the ν_e regeneration effect in the Earth [3,4] would be a spectacular, solar-model-independent confirmation of this theory (for reviews, see [5,6]).

The available data from the real-time solar neutrino experiment at Kamioka [7,8] are consistent with no Earth regeneration effect within the quoted uncertainties. This information can be used to exclude a region of the neutrino mass-mixing parameters in fits to the solar neutrino data [9–11].

A larger region of oscillation parameters relevant for the Earth effect will be probed by the new generation of solar neutrino experiments (as shown, e.g., in [12,13]). In particular, the SuperKamiokande experiment [14] (running) and the Sudbury Neutrino Observatory (SNO) experiment [15] (in construction) are expected to probe possible day-night modulations of the solar neutrino flux with unprecedented statistics and accuracy. A correct interpretation of the forthcoming high-quality data will demand precision calculations of the Earth-related observables.

The calculation of the Sun-Earth ν_e survival probability $P_{SE}(\nu_e)$ is based on the relation (Mikheyev and Smirnov, in [4])

$$P_{SE}(\nu_e) = P_S(\nu_e) + \frac{[2P_S(\nu_e) - 1][\sin^2\theta - P_E(\nu_2 \to \nu_e)]}{\cos 2\theta}, \tag{1}$$

where $P_S(\nu_e)$ is the ν_e survival probability at the Earth surface (or daytime probability), $P_E(\nu_2 \to \nu_e)$ is the probability of the transition from the mass state ν_2 to ν_e along the neutrino path in the Earth, and θ is the vacuum mixing angle.[1]

The calculation of P_E is notoriously difficult. Since the electron density in the Earth is not a simple function of the radius, the MSW equations have to be integrated numerically, unless stepwise approximations are adopted at the price of lower precision. Moreover, P_E must be averaged over given intervals of time:

---

[1] The derivation of Eq. (1) is reported in Appendix A for completeness.

$$\langle P_E \rangle = \frac{\int_{\tau_{d_1}}^{\tau_{d_2}} d\tau_d \int_{\tau_{h_1}(\tau_d)}^{\tau_{h_2}(\tau_d)} d\tau_h P_E(\eta(\tau_d, \tau_h))}{\int_{\tau_{d_1}}^{\tau_{d_2}} d\tau_d \int_{\tau_{h_1}(\tau_d)}^{\tau_{h_2}(\tau_d)} d\tau_h}, \tag{2}$$

where τ_d and τ_h are the daily and hourly times, respectively, and η is the nadir angle of the Sun at the detector site. In typical applications, the interval $[\tau_{d_1}, \tau_{d_2}]$ covers one year and the intervals $[\tau_{h_1}(\tau_d), \tau_{h_2}(\tau_d)]$ cover the nights, but other choices are possible.

The integration in Eq. (2) is time consuming. For instance, the authors of Refs. [9] and [10] quote a grid of about 30×30 integration points in the (year) × (night) domain, which requires massive calculations for spanning the relevant region of neutrino mass and mixing parameters with acceptable precision. The issue of numerical accuracy and stability is not secondary, since coarser integrations may generate fuzzy and misleading results (see, e.g., Fig. 5 of [16]).

A faster and more elegant method for averaging P_E consists in transforming the double integral of Eq. (2) into a single integral of the form

$$\langle P_E \rangle = \int_{\eta_1}^{\eta_2} d\eta\, W(\eta) P_E(\eta), \tag{3}$$

where the weight function $W(\eta)$ represents the "solar exposure" of the trajectory corresponding to the nadir angle η. This method was used by Cherry and Lande [4] for calculating the day-night asymmetry at the Homestake site. We have used this approach in our previous works [11] by computing numerically the Jacobian $d\tau/d\eta$ required to transform Eq. (2) into Eq. (3).

In this paper we show that, actually, the weight function $W(\eta)$ can be calculated analytically in several cases of practical interest. Moreover, we show that P_E can also be calculated analytically through a simple approximation which is more accurate than is required by the present (imperfect) knowledge of the Earth's interior. Within this approach, we work out the calculation of several solar-model-independent observables for the SuperKamiokande and SNO experiments in a two-family oscillation scenario.

Our work is organized as follows. In Sec. II we present the parametrization of the electron density. In Secs. III and

TABLE I. Coefficients of the electron density parametrization $N_j(r) = \alpha_j + \beta_j r^2 + \gamma_j r^4$, $[N] = \text{mol/cm}^3$, for the jth shell range $[r_{j-1}, r_j]$. The radial distance r is normalized to the Earth radius. See Fig. 1 for a plot of $N(r)$.

j	Shell	$[r_{j-1}, r_j]$	α_j	β_j	γ_j
1	Inner core	[0, 0.192]	6.099	-4.119	0.000
2	Outer core	[0.192, 0.546]	5.803	-3.653	-1.086
3	Lower mantle	[0.546, 0.895]	3.156	-1.459	0.280
4	Transition zone	[0.895, 0.937]	-5.376	19.210	-12.520
5	Upper mantle	[0.937, 1]	11.540	-20.280	10.410

IV we discuss the analytic calculation of P_E and W, respectively. In Sec. V we apply these calculations to the SuperKamiokande and SNO experiments. We draw our conclusions in Sec. VI. In order to make this work as self-contained and useful as possible, we organize in Appendixes A–C the relevant mathematical proofs. The reader interested mainly in the final results for SuperKamiokande and SNO may skip Secs. II–IV and the Appendixes, and read only Sec. V.

II. PARAMETRIZING THE EARTH ELECTRON DENSITY

In solar neutrino physics, the ''standard electroweak model'' of particle physics and the ''standard solar model'' of astrophysics must be supplemented by a ''standard Earth model'' of geophysics, such as the preliminary Earth reference model (PREM) of Dziewonski and Anderson [17]. This seemingly ''preliminary'' model elaborated in 1981 still represents the standard framework for the interpretation of seismological data,[2] as far as possible shell asphericities are neglected [19].

Eight shells are identified in the PREM model, but for any practical purpose related to solar neutrinos the four outer shells can be grouped into a single one (the ''upper mantle''). The Earth matter density profile $\rho(r)$ is given in detail in Table I of [17].

We have derived the electron density profile $N(r)$ from $\rho(r)$ by assuming the following chemical compositions (in weight): (1) mantle, SiO_2 (45.0%), Al_2O_3 (3.2%), FeO (15.7%), MgO (32.7%), and CaO (3.4%) [20]; (2) Core, Fe (96%) and Ni (4%) [21]. It follows that

$$N/\rho = \begin{cases} 0.494 & \text{(mantle)}, \\ 0.466 & \text{(core)}. \end{cases} \quad (4)$$

Figure 1 shows the five relevant Earth shells (in scale) and the electron density $N(r)$, together with the basic geometry that will be used in the following sections. For each shell j, we use a polynomial fit that approximates accurately the true radial density,

$$N_j(r) = \alpha_j + \beta_j r^2 + \gamma_j r^4, \quad (5)$$

where the coefficients α_j, β_j, and γ_j are given in Table I.

The functional form in Eq. (5) is invariant for nonradial ($\eta \neq 0$) neutrino trajectories:

$$N_j(x) = \alpha'_j + \beta'_j x^2 + \gamma'_j x^4, \quad (6)$$

where

$$\alpha'_j = \alpha_j + \beta_j \sin^2 \eta + \gamma_j \sin^4 \eta, \quad (7a)$$

$$\beta'_j = \beta_j + 2\gamma_j \sin^2 \eta, \quad (7b)$$

$$\gamma'_j = \gamma_j, \quad (7c)$$

with the trajectory coordinate x and the nadir angle η defined as in Fig. 1.

For later purposes it is useful to split the density (in each shell and for each trajectory) as

$$N_j(x) = \bar{N}_j + \delta N_j(x), \quad (8)$$

where $\bar{N}$ is the (η-dependent) average density along the shell chord,

$$\bar{N}_j = \int_{x_{j-1}}^{x_j} dx N_j(x) \Big/ (x_j - x_{j-1}), \quad (9)$$

and $\delta N_j(x)$ is the residual density variation. It will be seen that the above parametrization of $N(x)$ plays a basic role in the analytic calculation of the neutrino probability P_E.

We end this section with an estimate of the likely uncertainties affecting $N(x)$. The core, which is usually assumed to be iron dominated, could contain a large fraction of lighter elements without necessarily conflicting with the seismological data. An example is given by a model of core made of Fe (55%) and FeO (45%) [18], which would increase N by 0.65%. Concerning the mantle, alternative chemical compositions (see Table 4 in [20]) typically reduce N by 1–2%. We will evaluate the effect of representative density uncertainties by varying N by $+1\%$ in the core and by -1.5% in the mantle. However, these error estimates might be optimistic, according to Birch's old admonition [22].

III. CALCULATING P_E WITH ELEMENTARY FUNCTIONS

In this section we show that the probability $P_E(\nu_2 \rightarrow \nu_e)$ can be accurately approximated by elementary analytic expressions. We start by observing that P_E can be expressed as

$$P_E = |\mathcal{U}_{ee} \sin\theta + \mathcal{U}_{e\mu} \cos\theta|^2, \quad (10)$$

---

[2]For a review of recent progress in the study of the Earth interior, see also [18].

I = ν entry point
F = ν end point (detector)
M = trajectory midpoint
P = generic ν position
x = MP = trajectory coordinate
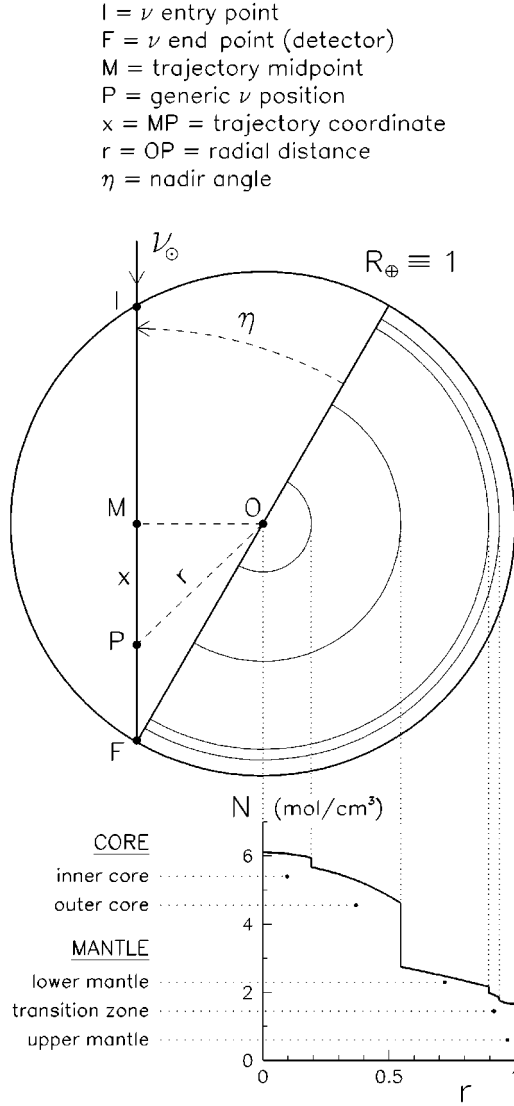r = OP = radial distance
η = nadir angle

FIG. 1. Section of the Earth showing the relevant shells (in scale) and the electron density profile $N(r)$. The geometric definitions used in the text are also displayed.

where $\mathcal{U}$ is the neutrino evolution operator in the (ν_e, ν_μ) flavor basis.

In the same flavor basis, the MSW Hamiltonian $\mathcal{H}_j(x)$ along the jth shell chord traversed by the neutrino is given by

$$\mathcal{H}_j(x)$$
$$= \frac{1}{2}\begin{pmatrix} \sqrt{2}G_F N_j(x) - k\cos 2\theta & k\sin 2\theta \\ k\sin 2\theta & k\cos 2\theta - \sqrt{2}G_F N_j(x) \end{pmatrix},$$
(11)

where $k = \delta m^2/2E_\nu$ is the vacuum oscillation wave number, $N_j(x)$ is the electron density as in Eq. (6), and δm^2, θ, and E_ν are the neutrino mass square difference, mixing angle, and energy, respectively.

Following Eq. (8), we split the Hamiltonian into a constant matrix plus a perturbation:

$$\mathcal{H}_j(x) = \overline{\mathcal{H}}_j + \delta\mathcal{H}_j(x),$$
(12)

where $\overline{\mathcal{H}}_j = \mathcal{H}_j|_{N\to\overline{N}}$, and $\delta\mathcal{H}_j(x) = G_F/\sqrt{2}\,\mathrm{diag}[\delta\underline{N}_j(x), -\delta N_j(x)]$. Notice that the unperturbed Hamiltonian $\overline{\mathcal{H}}_j$ depends on the nadir angle η through $\overline{N}_j$.

We have worked out explicitly, at the first perturbative order, the evolution operator $\mathcal{U}_j$ for the jth shell chord in the flavor basis. The result is

$$\mathcal{U}_j(x_j, x_{j-1}) = e^{-i\overline{\mathcal{H}}_j(x_j - x_{j-1})} - i\int_{x_{j-1}}^{x_j} dx\, e^{-i\overline{\mathcal{H}}_j(x_j - x)}\delta\mathcal{H}_j(x)$$
$$\times e^{-i\overline{\mathcal{H}}_j(x - x_{j-1})} + O(\delta\mathcal{H}_j^2)$$
$$= \begin{pmatrix} c_j + is_j\cos 2\overline{\theta}_m & -is_j\sin 2\overline{\theta}_m \\ -is_j\sin 2\overline{\theta}_m & c_j - is_j\cos 2\overline{\theta}_m \end{pmatrix}$$
$$- \frac{i}{2}\sin 2\overline{\theta}_m$$
(13)

$$\times \begin{pmatrix} C_j\sin 2\overline{\theta}_m & C_j\cos 2\overline{\theta}_m - iS_j \\ C_j\cos 2\overline{\theta}_m + iS_j & -C_j\sin 2\overline{\theta}_m \end{pmatrix}$$
$$+ O(\delta\mathcal{H}_j^2),$$
(14)

where $\overline{\theta}_m$ is the average mixing angle in matter,

$$\sin 2\overline{\theta}_m/\sin 2\theta = [(\cos 2\theta - \sqrt{2}G_F\overline{N}_j/k)^2 + \sin^2 2\theta]^{-1/2},$$
(15)

and

$$c_j = \cos[\overline{k}_m(x_j - x_{j-1})/2],$$
(16a)

$$s_j = \sin[\overline{k}_m(x_j - x_{j-1})/2],$$
(16b)

$$C_j = \sqrt{2}G_F\int_{x_{j-1}}^{x_j} dx\,\delta N_j(x)\cos\overline{k}_m(x - \overline{x}),$$
(16c)

$$S_j = \sqrt{2}G_F\int_{x_{j-1}}^{x_j} dx\,\delta N_j(x)\sin\overline{k}_m(x - \overline{x}),$$
(16d)

with $\overline{k}_m = k\sin 2\theta/\sin 2\overline{\theta}_m$ (average matter oscillation wave number) and $\overline{x} = (x_j + x_{j-1})/2$ (shell chord midpoint).

The integrals in Eqs. (16c) and (16d) are elementary, δN_j being a (biquadratic) polynomial in x (see Sec. II). The property $\int_{x_{j-1}}^{x_j} dx\,\delta N_j(x) = 0$, which follows from Eqs. (8) and (9), is crucial for obtaining the compact expression of $\mathcal{U}_j$ in Eq. (14).

The evolution operator along the total neutrino path $\overline{IF}$ (see Fig. 1) is simply given by the ordered product of the partial evolution operators along the shell chords, $\mathcal{U}(x_F, x_I) = \Pi_j\mathcal{U}(x_j, x_{j-1})$. Actually, because of the symmetry of the electron density with respect to the trajectory midpoint M, one needs only to calculate the evolution operator from $x_M(=0)$ to $x_F(=-x_I)$:

$$\mathcal{U}(x_F, x_I) \equiv \mathcal{U}(x_F, 0)\cdot\mathcal{U}(0, -x_F) = \mathcal{U}(x_F, 0)\cdot\mathcal{U}^T(x_F, 0).$$
(17)

The proof of the above property is given in Appendix B.
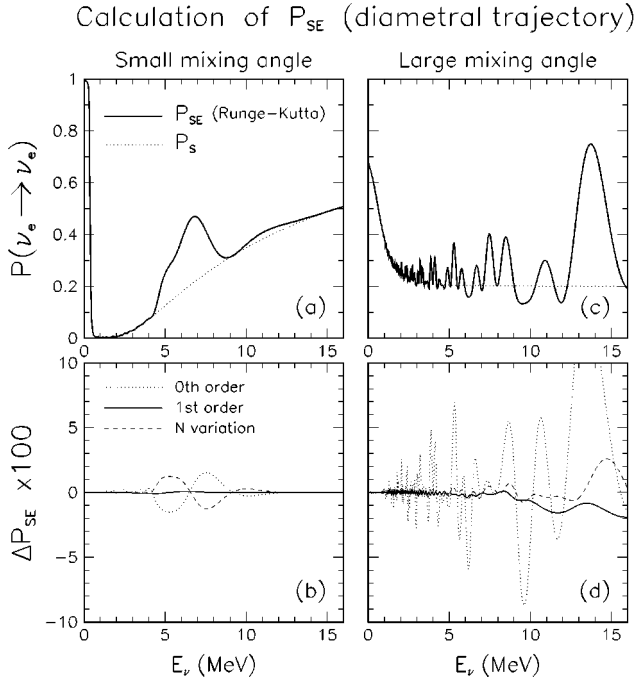
Calculation of P_{SE} (diametral trajectory)

FIG. 2. Comparison of different calculations of $P_{SE}(E_\nu)$ for ^{8}B neutrinos crossing the Earth diameter. (a) Calculation of P_{SE} with Runge-Kutta integration for the small-mixing angle case (solid line). Also shown is the function P_S (dotted line). (b) Variations of P_{SE} induced by representative density shifts (dashed line), and by the first-order and zeroth-order approximations discussed in the text (solid and dotted line, respectively). Panels (c) and (d) are analogous to (a) and (b), but refer to the large-mixing angle case.

So far we have solved analytically the MSW equations in the Earth at first order in perturbation theory, by expressing the total evolution operator $\mathcal{U}$ in the flavor basis as a product of matrices (one for each shell traversed in a semitrajectory) involving only elementary functions. The desired probabilities P_E and P_{SE} are then given by Eqs. (10) and (1), respectively. Now we discuss the accuracy of such first-order approximation.

Figure 2 shows, for two representative mass-mixing scenarios and for diametral crossing, the results of various approximations of P_{SE} as a function of the neutrino energy. Figures 2(a) and 2(b) refer to the small mixing angle solution to the solar neutrino problem, corresponding to $(\delta m^2/\mathrm{eV}^2, \sin^2 2\theta) \simeq (5.2 \times 10^{-6}, 8.1 \times 10^{-3})$ [11]. In Fig. 2(a), the probability P_S (dotted line) is calculated semianalytically [11] and averaged over the ^{8}B production region in the Sun [23] (as required for applications to SuperKamiokande and SNO). The probability P_{SE} in Fig. 2(a) (thick, solid line) has been obtained by integrating the MSW equations in the Earth with the highest possible accuracy, i.e., with a Runge-Kutta method and with the true (PREM) electron density. In Fig. 2(b) we show the residuals ΔP_{SE} of different calculations with respect to the "Runge-Kutta" P_{SE}. The solid curve in Fig. 2(b) refers to the first-order perturbative approach discussed in this section. The dotted curve is obtained by using the simple zeroth-order approximation (i.e., average density shells). The dashed curve shows the variations of P_{SE} induced by plausible uncertainties in the electron density N (as discussed at the end of Sec. II). It can be seen that the effect of the latter uncertainties is com-

parable to the errors associated with the zeroth-order approximation, and is much larger than the errors of the first-order approximation.

Figures 2(c) and 2(d) are analogous of Figs. 2(a) and 2(b) for the large mixing angle solution to the solar neutrino problem, corresponding to $(\delta m^2/\mathrm{eV}^2, \sin^2 2\theta) \simeq (1.5 \times 10^{-5}, 0.64)$ [11]. It can be seen that the errors associated with the first-order approximation are generally smaller than the effect of the N uncertainties, which are in turn much smaller than the errors of the zeroth-order approximation.

The results of Fig. 2 and of many other checks that we have performed for different values of $(\delta m^2, \sin^2 2\theta)$ and η show that the analytic (first-order) solution discussed in this section represents a very good approximation to the true electron survival probability in the Earth, with an accuracy better (often much better) than is required by the likely uncertainties affecting the Earth electron density.

Finally, we point out that our analytic approximation for the neutrino evolution operator in the Earth matter can be applied also in the analysis of atmospheric neutrinos, and that its computer evaluation is much faster (about two orders of magnitude) than typical Runge-Kutta numerical integrations.

IV. WEIGHTING NEUTRINO TRAJECTORIES

As anticipated in the Introduction, the time average of the neutrino regeneration probability in the Earth [Eq. (2)] can be transformed into a (more manageable) weighted average over the trajectory nadir angle η [Eq. (3)], with a weight function $W(\eta)$ having a compact, analytic form in several cases of practical interest. In this section we describe the results for the important case of annual averages during (a fraction of) night. We refer the reader to Appendix C for mathematical proofs and for a discussion of other cases.

The weight function $W(\eta)$ for annual averages is presented in Table II. In different ranges of the detector latitude λ and of the nadir angle η, $W(\eta)$ takes different functional forms, involving the calculation of a complete elliptic integral of the first kind [24,25] (which is coded in many computer libraries; see, e.g., [26]).

In Fig. 3 the function $W(\eta)$ is plotted for the SuperKamiokande and SNO latitudes. The area under each curve is equal to 1. We show $W(\eta)$ also for the Gran Sasso site, relevant for several proposed solar neutrino projects such as the Borexino experiment [27], the Imaging of Cosmic And Rare Underground Signals (ICARUS) experiment [28], the permanent Gallium Neutrino Observatory (GNO) [29], and the Helium at Liquid Azote temperature (HELLAZ) detector [30]. Finally, the dotted line in Fig. 3 represents the weight function for a hypothetical detector located at the equator, where the Earth regeneration effect would be more sizable [31]. The divergence of $W(\eta)$ is logarithmic and thus it is integrated out by binning in η. Several methods exist for dealing with the numerical quadrature of divergent integrands [32].

By using $W(\eta)$ as given in Table II (or in Fig. 3), the average probability during night simply reads

$$\langle P_E \rangle_{\mathrm{night}} = \int_0^{\pi/2} d\eta \, W(\eta) P_E(\eta). \tag{18}$$

TABLE II. Weight function $W(\eta)$ for annual averages at the latitude λ (i denotes the Earth inclination). $W(\eta)$ takes different functional forms in the indicated ranges of η and λ. K is the complete elliptic function of the first kind, with arguments defined in the bottom row.

Weight function	Ranges of detector latitude λ and nadir angle η		
$W(\eta)$ for annual averages	Equator to tropic $(0 \leq \lambda \leq i)$	Tropic to polar circle $(i < \lambda \leq \pi/2 - i)$	Polar circle to pole $(\pi/2 - i < \lambda \leq \pi/2)$
0	—	$0 \leq \eta < \lambda - i$	$0 \leq \eta \leq \lambda - i$
$\dfrac{2\sin\eta}{\pi^2 z} K(y/z)$	$i - \lambda < \eta < i + \lambda$	$\lambda - i \leq \eta < \lambda + i$	$\lambda - i \leq \eta < \pi - \lambda - i$
$\dfrac{2\sin\eta}{\pi^2 y} K(z/y)$	$0 \leq \eta < i - \lambda$, or $i + \lambda < \eta \leq \pi/2$	$\lambda + i < \eta \leq \pi/2$	$\pi - \lambda - i < \eta \leq \pi/2$
Definitions:	$z = \sqrt{\sin i \cos\lambda \sin\eta}$, $y = \sqrt{\sin\dfrac{i+\lambda+\eta}{2}\sin\dfrac{i-\lambda+\eta}{2}\cos\dfrac{i+\lambda-\eta}{2}\cos\dfrac{i-\lambda-\eta}{2}}$		

The annual average during the fractions of night in which the Earth core is crossed has also a particular relevance as emphasized, e.g., in [12,31]. With the weight method, it can be easily calculated as

$$\langle P_E \rangle_{\text{core}} = \frac{\displaystyle\int_0^{\eta_{\text{core}}} d\eta\, W(\eta) P_E(\eta)}{\displaystyle\int_0^{\eta_{\text{core}}} d\eta\, W(\eta)}, \qquad (19)$$

where $\eta_{\text{core}}(=0.577 \text{ rad})$ is the nadir angle subtending the Earth (inner and outer) core.

A final remark is in order. In the expression for the time average [Eq. (2)] we have not included the geometric factor L^{-2} accounting for the neutrino flux variations with the Earth-Sun distance L. We have implicitly assumed that the data from the real-time SuperKamiokande and SNO experi-

ments will be corrected for this factor in any period of data taking. The effect of dropping this assumption is examined in Appendix D. We anticipate that, for annual averages, the effect is less than 1%.

V. CALCULATING SOLAR-MODEL-INDEPENDENT OBSERVABLES

The SuperKamiokande and SNO experiments are sensitive only to the high-energy part of the solar neutrino spectrum, namely, to ^{8}B neutrinos. Since the estimated uncertainty of the theoretical ^{8}B neutrino flux Φ_B is relatively large ($\sim 16\%$ at 1σ [23]), it is important to focus on observables that do not depend on the absolute value of Φ_B, but are sensitive only to the *shape* of the ^{8}B energy spectrum, which is rather well known from laboratory measurements [33].[3] Important examples of these quantities are the night-day rate asymmetry, the shape distortions of the angular spectrum, and the shape distortions of the recoil electron energy spectrum. The SNO experiment can measure, in addition, the charged-to-neutral current event ratio, which is also solar-model independent. In this section we calculate the annual averages of several such observables, by including the Earth effect with the method described in the previous sections.

We take from [35] the neutrino interaction cross sections for SuperKamiokande. The effects of the detector energy resolution and threshold are included as in [36,37] (see, in particular, Table I of [36] for the detector technical specifications). Concerning the distortions of the electron energy spectra due to neutrino oscillations, we adopt, as in [36], the approach in terms of the first two moments of the electron energy distribution, namely, the average electron kinetic energy $\langle T \rangle$ and the variance σ^2 of the energy spectrum. The reader is referred to [36] for an extensive discussion of the spectral moments and for an estimate of their likely uncertainties.

A. SuperKamiokande

Figure 4 shows the nadir angle (η) distribution of events expected at SuperKamiokande. We use the same format (five
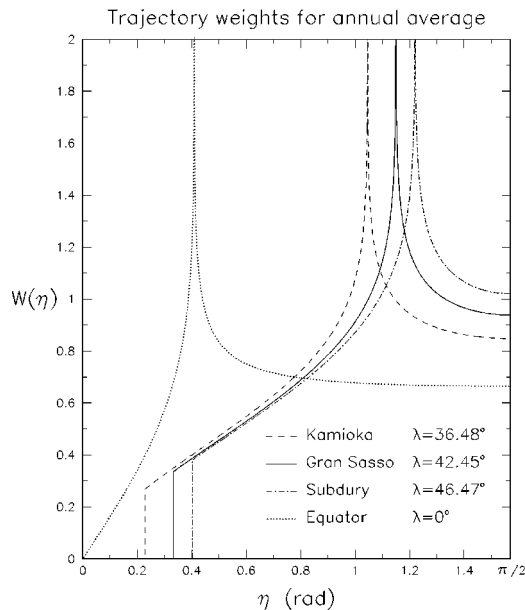

FIG. 3. Annual solar exposure (weight) of the trajectory at nadir angle η for representative values of the latitude λ. See the text for details.

---

[3]It is also well established that the laboratory and solar ^{8}B neutrino spectra are the same to high accuracy [34].
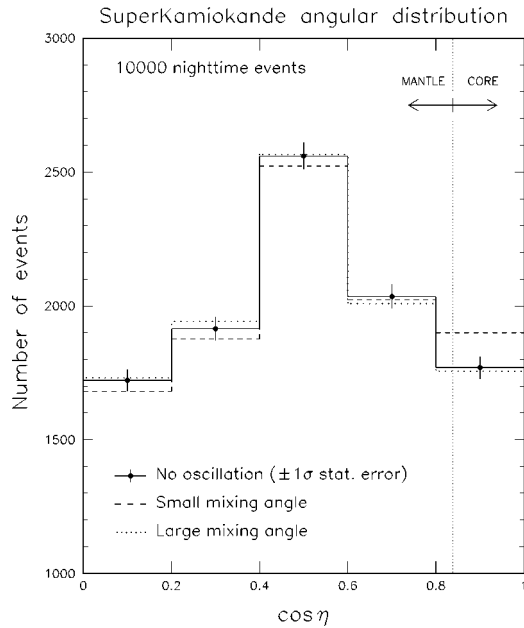
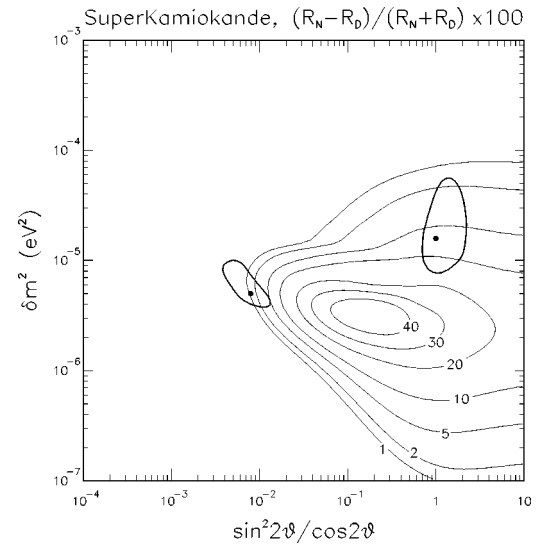FIG. 4. Nadir angle distribution of night-time events at SuperKamiokande. Error bars are statistical only.

FIG. 5. Night-day asymmetry of neutrino rates at SuperKamiokande. The best-fit points and the 90% C.L. regions for the small- and large-mixing angle solutions are superposed.
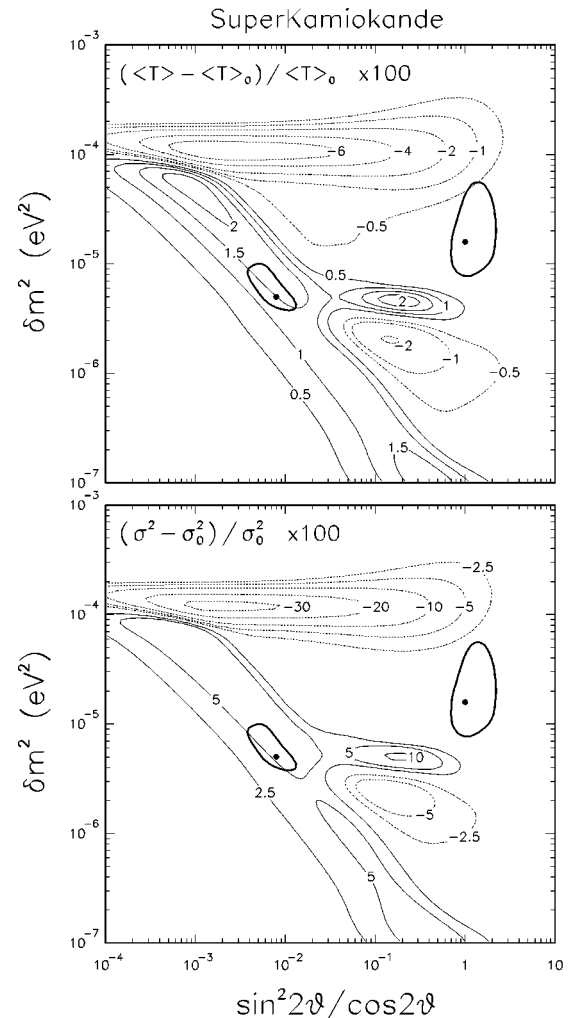

FIG. 6. Fractional deviations of the first two moments of the SuperKamiokande electron energy distribution ($\langle T \rangle$ and σ^2) from their no-oscillation values ($\langle T \rangle_0$ and σ_0^2).

bins in $\cos\eta$) as the Kamiokande experiment [7]. The solid line is the distribution expected in the absence of oscillations, which is simply obtained by integrating the weight function of Fig. 3 in each bin of $\cos\eta$. The dashed and dotted histograms refer to the (best-fit) small-mixing and large-mixing solutions, respectively. All histograms are normalized to the same number of events in order to make the relative deviations independent of the absolute neutrino flux. Assuming a statistics of 10 000 night-time events, the small-mixing angle case appears to be separated by $\sim 3\sigma$ (statistical errors only) from the no oscillation case in the last bin, which collects neutrinos crossing the Earth core. In fact, in the small-mixing angle case there is a strong regeneration effect in the core (see, e.g., [12]). In the (best-fit) large-mixing angle case, instead, the sudden variations of P_{SE} with η [12] happen to be smeared by binning and the net deviations are smaller (the effect, however, is very sensitive to the specific mass-mixing parameters chosen). Preliminary results from SuperKamiokande [38] indicate a rate of ~ 10 event/day above 7 MeV. This translates into ~ 20 event/day for the prospected 5 MeV threshold. Therefore, about three years of operation will be required to collect 10^4 night-time events.

Figure 5 shows the night-day asymmetry of neutrino rates, which is perhaps the most popular characterization of the Earth effect. The 90% C.L. regions corresponding to the small- and large-mixing angle solution [11] are superposed to curves of equal values of the asymmetry. Similar results have been obtained by Krastev in [13]. Notice that asymmetry measurements at the percent level would allow a complete (partial) exploration of the large- (small-)mixing angle solution.

Figure 6 shows the fractional deviations in the first two moments of the electron energy distribution ($\langle T \rangle$ and σ^2) with respect to their no oscillation values ($\langle T \rangle_0$ and σ_0^2). These deviations represent a useful characterization of spectral distortions [36]. The deviations expected for the small-mixing angle solution [36], although significant, are

SuperKamiokande

$(\langle T\rangle_N - \langle T\rangle_D)/\langle T\rangle \ \times 100$

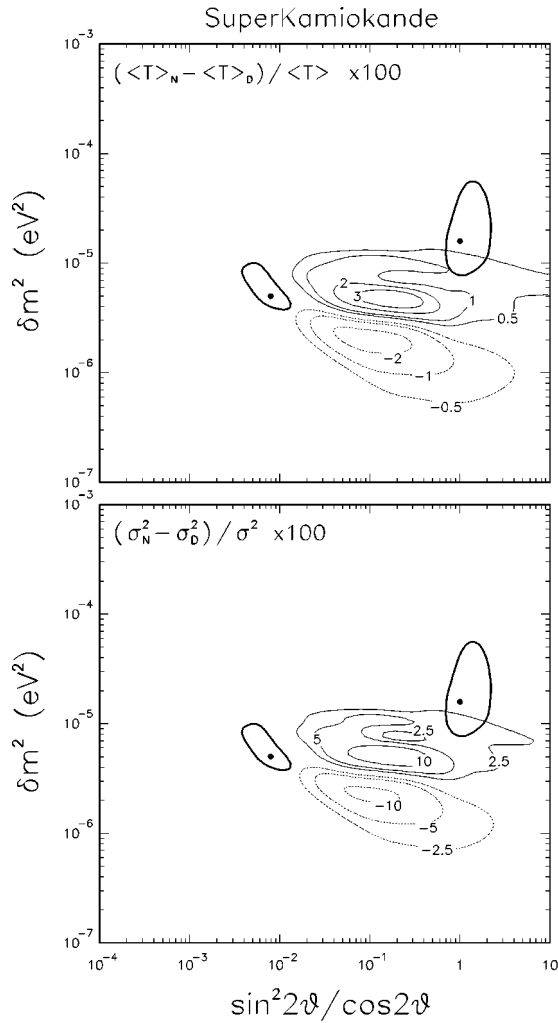$(\sigma_N^2 - \sigma_D^2)/\sigma^2 \ \times 100$

FIG. 7. Night-day fractional variations of the spectral moments at SuperKamiokande.

only slightly affected by the Earth effect. The deviations for the large angle solution are very small. In the region of "intermediate" mixing there could be strong, Earth-related deformations of the spectrum. Calculations of $\langle T\rangle$ including the Earth effect were first presented in [10]. A comparison of their Fig. 5 [10] with our Fig. 6 shows once again that the accuracy and stability of numerical calculations of the Earth effect are important issues. We obtain results very similar to those in Ref. [36] when the Earth effect is switched off.[4]

Figure 7 shows the night-day variation of the spectral moments at SuperKamiokande. The relative deviations of the night-time (N) and daytime (D) values of $\langle T\rangle$ and σ^2 characterize the daily deformations of the electron spectrum due to neutrino oscillations in the Earth matter (averaged over the year). For $\delta m^2 \gtrsim 3\times10^{-6}$ eV^2 ($\delta m^2 \lesssim 3\times10^{-6}$ eV^2) the Earth effect tends to increase the rate in the high-energy (low-energy) part of the electron spectrum. This explains the sign of the night-day spectral deviations in Fig. 7. Therefore, if a significant Earth effect were observed, the sign of these deviations could provide an additional handle for discriminating the value of δm^2.

---

[4]It is worth mentioning that the computer codes used in this work are independent from those used in [36].

SNO angular distribution

10000 nighttime events

MANTLE CORE

No oscillation ($\pm 1\sigma$ stat. error)
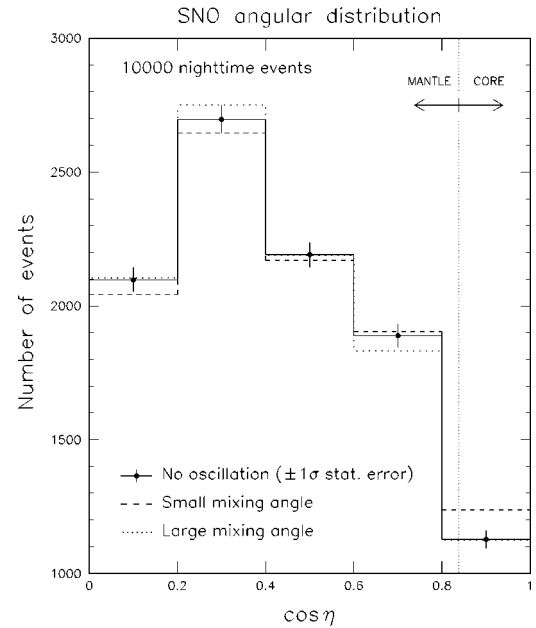Small mixing angle
Large mixing angle

FIG. 8. Nadir angle distribution of night-time events at SNO. Error bars are statistical only.

B. SNO

The results of our calculation of the angular distribution, day-night asymmetry, and spectral deviations for the SNO experiments are presented in Figs. 8–11. These figures are analogous to Figs. 4–7 for SuperKamiokande, and similar comments apply. We just add that, in general, the various Earth-related effects appear to be more significant in SNO than in SuperKamiokande, as a result of the intrinsically higher correlation between the (observed) electron energy and the (unknown) neutrino energy. However, since the event rate in SNO is expected to be a factor ~ 0.6 lower than that in SuperKamiokande, the statistics of 10^4 night-time events indicated in Fig. 8 will require about five years of data taking.

In addition, the SNO experiment will separate events produced in charged current (CC) interactions of ν_e's from

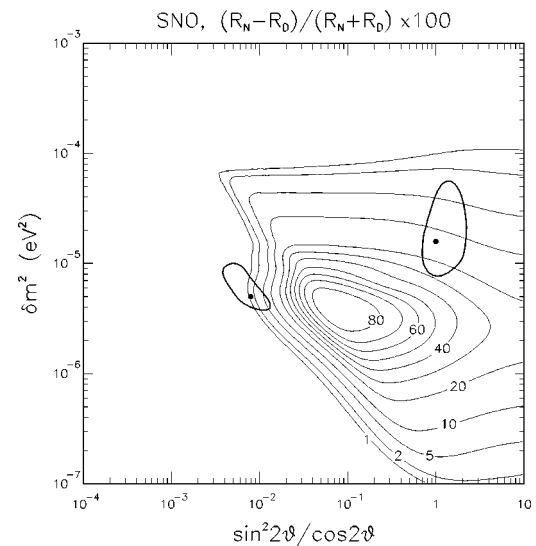## SNO, $(R_N - R_D)/(R_N + R_D) \times 100$

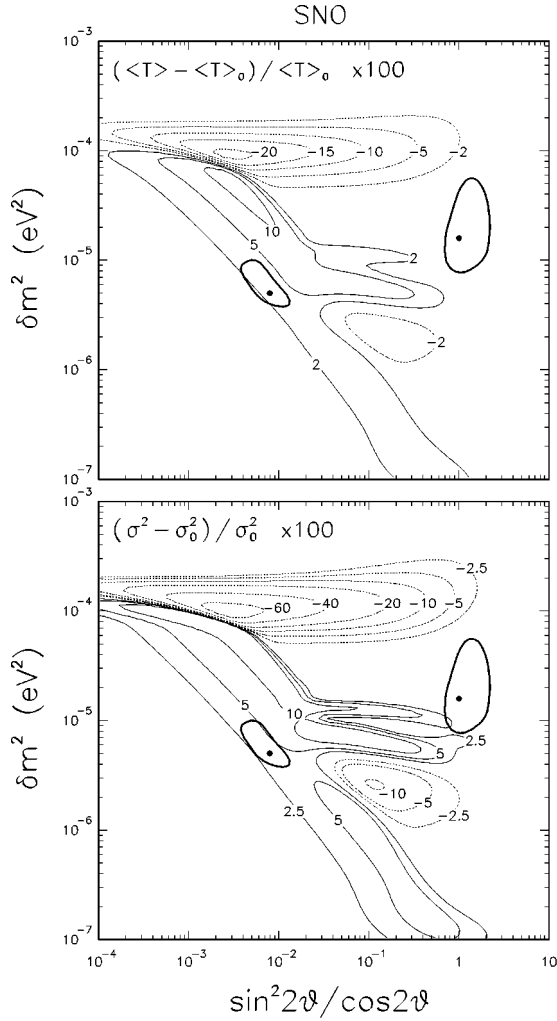FIG. 9. Night-day asymmetry of neutrino rates at SNO.

FIG. 10. Fractional deviations of the first two moments of the SNO electron energy distribution ($\langle T \rangle$ and σ^2) from their no-oscillation values.

FIG. 11. Night-day fractional variations of the spectral moments at SNO.

events produced in neutral current (NC) interactions of neutrinos of all flavors. The ratio of the CC and NC rates is perhaps the most crucial, solar-model-independent observable that will be measured in the next few years. Curves of the CC/NC ratio, including the Earth effect, are shown in Fig. 12. The value expected for no oscillation (indicated in the left, lower corner) agrees with the value given in [36]. Notice that we have taken the efficiencies for detecting CC and NC events (ε_{CC} and ε_{NC}, respectively) equal to 100%. When the true experimental efficiencies will be known, the values in Fig. 12 should be multiplied by $\varepsilon_{CC}/\varepsilon_{NC}$.

VI. CONCLUSIONS

The observation of solar neutrino oscillations enhanced by the Earth matter would be a spectacular confirmation of the MSW theory. The new generation of solar neutrino experiments can probe this possibility with unprecedented accuracy. In particular, the interpretation of the forthcoming, high-quality data from the SuperKamiokande and SNO experiments demands precision calculations of the Earth effect in solar neutrino oscillations.

We have presented an analytic method for approximating the ν_e regeneration probability in the Earth, based on a first-
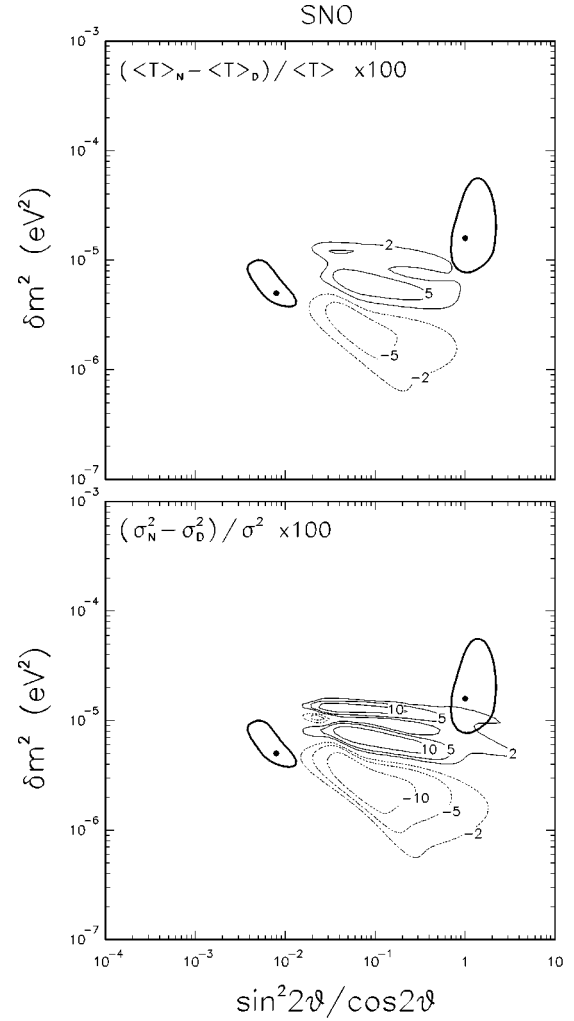
order perturbative expansion of the MSW Hamiltonian and on a convenient parametrization of the Earth electron density. We have also shown how time averages of the ν_e sur-
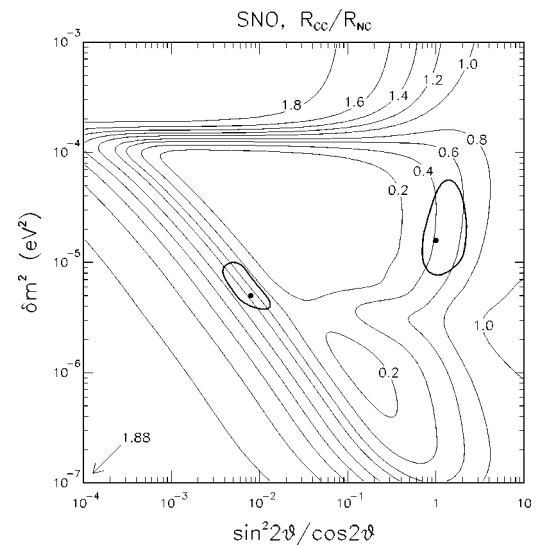

FIG. 12. Ratio of charged current to neutral current neutrino interactions at SNO.

vival probability can be transformed into weighted averages over the nadir angle, with weights that can be calculated analytically in several relevant cases. Mathematical proofs and final results are described in detail, especially for the case of annual averages.

We have then calculated accurately the following solar-model-independent observables for the SuperKamiokande and SNO experiments: (1) the angular distribution of events; (2) the night-day asymmetry of the neutrino rates; (3) the fractional deviations of the first two spectral moments of the electron energy distribution; (4) the night-day fractional variations of such moments; and (5) the charged-to-neutral current event ratio for SNO.

The approach to the Earth effect presented in this paper allows simpler, faster, and more versatile calculations than brute-force integration methods. We hope that these advantages may lead more people to try a do-it-yourself analysis of the Earth regeneration effect in solar neutrino oscillations.

APPENDIX A: THE SUN-EARTH SURVIVAL PROBABILITY P_{SE}

In this appendix we report, for the sake of completeness, the derivation of Eq. (1) (Mikheyev and Smirnov, in [4]). A solar neutrino arriving at Earth in the flavor state ν_α is an incoherent mixture of vacuum mass states ν_i. The corresponding probabilities $P_S(\nu_\alpha)$ and $P_S(\nu_i)$ are then given by

$$\begin{bmatrix} P_S(\nu_e) \\ P_S(\nu_\mu) \end{bmatrix} = \begin{bmatrix} \cos^2\theta & \sin^2\theta \\ \sin^2\theta & \cos^2\theta \end{bmatrix} \begin{bmatrix} P_S(\nu_1) \\ P_S(\nu_2) \end{bmatrix}. \quad \text{(A1)}$$

The probability $P_{\text{SE}}(\nu_\alpha)$ that a solar neutrino has flavor α after traversing the Earth can be expressed as

$$\begin{bmatrix} P_{\text{SE}}(\nu_e) \\ P_{\text{SE}}(\nu_\mu) \end{bmatrix} = \begin{bmatrix} 1 - P_E(\nu_2 \to \nu_e) & P_E(\nu_2 \to \nu_e) \\ P_E(\nu_2 \to \nu_e) & 1 - P_E(\nu_2 \to \nu_e) \end{bmatrix} \begin{bmatrix} P_S(\nu_1) \\ P_S(\nu_2) \end{bmatrix}, \quad \text{(A2)}$$

where P_E is the probability of the $\nu_2 \to \nu_e$ transition in the Earth. Equation (1) follows then from Eqs. (A1) and (A2).

The incoherence of neutrino mass state components in Eqs. (A1) and (A2) is guaranteed by at least three facts: (1) the neutrino production region in the Sun is an order of magnitude larger than the Earth radius; (2) for typical values of neutrino mass and mixing parameters, solar neutrinos oscillate many times in their Sun-Earth path, with final wave packet divergences larger than the oscillation wavelength; and (3) any detection process implies some energy smearing. A hypothetical coherent mixture would give rather different numerical results for P_{SE} [39].

APPENDIX B: PROOF OF THE PROPERTY $\mathcal{U}(0,-x) = \mathcal{U}^T(x, 0)$

Let us consider the Schrödinger equation

$$i \frac{d\psi(x)}{dx} = \mathcal{H}(x)\psi(x) \quad \text{(B1)}$$

and its formal solution

$$\psi(x) = \mathcal{U}(x, 0)\psi(0), \quad \text{(B2)}$$

where $\mathcal{U}$ is the evolution operator ($\mathcal{U}^\dagger \mathcal{U} = \mathbb{1}$).

If the Hamiltonian is real ($\mathcal{H} = \mathcal{H}^*$) and obeys the symmetry $\mathcal{H}(x) = \mathcal{H}(-x)$, then $\psi^*(-x)$ is also a solution of Eq. (B1):

$$\psi^*(-x) = \mathcal{U}(x, 0)\psi^*(0), \quad \text{(B3)}$$

that is,

$$\psi(0) = [\mathcal{U}^*(x, 0)]^{-1}\psi(-x) = \mathcal{U}^T(x, 0)\psi(-x), \quad \text{(B4)}$$

which implies that $\mathcal{U}(0, -x) = \mathcal{U}^T(x, 0)$.

APPENDIX C: CHANGING INTEGRATION MEASURE, $\int d\tau_d \int d\tau_h \to \int d\eta$

In this appendix we show how to transform an integral of the kind $\int d\tau_d \int d\tau_h$ into an integral of the kind $\int d\eta$. In particular, Eq. (18) is explicitly derived for a detector latitude between the tropic and the polar circle (see Table II). Other cases are discussed at the end of this appendix.

The daily and hourly times are conventionally normalized to the interval $[0, 2\pi]$:

$$\tau_d = \frac{\text{day}}{365} 2\pi, \quad \text{(C1)}$$

$$\tau_h = \frac{\text{hour}}{24} 2\pi, \quad \text{(C2)}$$

with $\tau_d = 0$ at the winter solstice and $\tau_h = 0$ at midnight. The nadir angle η, the daily time τ_d, and the hourly time τ_h, are linked by the relations

$$\cos\eta = \cos\lambda \cos\tau_h \cos\delta_S - \sin\lambda \sin\delta_S, \quad \text{(C3)}$$

$$\sin\delta_S = -\sin i \cos\tau_d, \quad \text{(C4)}$$

where λ is the detector latitude (in radiants), i is the Earth inclination ($i = 0.4091$ rad), and δ_S is the Sun declination. The sunrise (sr) and sunset (ss) times (corresponding to $\eta = \pm \pi/2$) are then given by $\tau_h^{\text{sr}} = \arccos(\tan\lambda \tan\delta_S)$ and $\tau_h^{\text{ss}} = -\tau_h^{\text{sr}}$, respectively.

The annual average during nights can be restricted, for symmetry, to one-half year and to one-half night (midnight-sunrise interval):

$$\langle P_E \rangle_{\text{night}} = \frac{\int_0^\pi d\tau_d \int_0^{\tau_h^{\text{sr}(\tau_d)}} d\tau_h P_E(\eta(\tau_d, \tau_h))}{\int_0^\pi d\tau_d \int_0^{\tau_h^{\text{sr}(\tau_d)}} d\tau_h}. \quad \text{(C5)}$$

The integral at the denominator in Eq. (C5) is trivial and gives $\pi^2/2$. The integral at the numerator in Eq. (C5) can be transformed as

$$\int_0^\pi d\tau_d \int_{\lambda+\delta_S}^{\pi/2} d\eta \frac{d\tau_h}{d\eta}(\tau_d,\eta) P_E(\eta)$$

$$= \int_{\lambda-i}^{\pi/2} d\eta P_E(\eta) \int_0^{\hat{\tau}_d(\eta)} d\tau_d \frac{d\tau_h}{d\eta}(\tau_d,\eta) \qquad \text{(C6)}$$

$$= \frac{\pi^2}{2} \int_0^{\pi/2} d\eta P_E(\eta) W(\eta), \qquad \text{(C7)}$$

where

$$\hat{\tau}_d(\eta) = \begin{cases} 0, & 0 \leq \eta < \lambda - i \\ \arccos\left(\frac{\sin(\lambda-\eta)}{\sin i}\right), & \lambda - i \leq \eta < \lambda + i \\ \pi, & \lambda + i \leq \eta \leq \pi/2, \end{cases} \qquad \text{(C8)}$$

and $W(\eta)$ is defined as

$$W(\eta) = \frac{2}{\pi^2} \begin{cases} 0, & 0 \leq \eta < \lambda - i, \\ \int_0^{\hat{\tau}_d(\eta)} d\tau_d \frac{d\tau_h}{d\eta}(\tau_d,\eta), & \lambda - i \leq \eta \leq \pi/2. \end{cases} \qquad \text{(C9)}$$

The interchange of integration variables in Eq. (C6) and the definition in Eq. (C8) can be understood by drawing the integration domain in the (τ_d,η) plane (not shown) for a detector latitude between the tropic and the polar circle $(i < \lambda \leq \pi/2 - i)$.

From Eqs. (C3) and (C4) one derives, after some algebra,

$$\int_0^{\hat{\tau}_d(\eta)} d\tau_d \frac{d\tau_h}{d\eta}(\tau_d,\eta)$$

$$= \frac{\sin\eta}{\sin i} \int_{\max\{p,-1\}}^1 \frac{d\xi}{\sqrt{(\xi+1)(\xi-1)(\xi-p)(\xi-q)}}, \qquad \text{(C10)}$$

where

$$p = \sin(\lambda - \eta)/\sin i, \qquad \text{(C11a)}$$

$$q = \sin(\lambda + \eta)/\sin i, \qquad \text{(C11b)}$$

$$\xi = \cos\tau_d. \qquad \text{(C11c)}$$

The right-hand side of Eq. (C10) can be expressed in terms of the complete elliptic integral of the first kind, defined as

$$K(x) = \int_0^1 \frac{ds}{\sqrt{(1-s^2)(1-x^2 s^2)}} \qquad \text{(C12)}$$

(see [24], pp. 241–243). The results in the third column of Table II are finally obtained with the positions

$$z = \sin i \sqrt{(q-p)/2}, \qquad \text{(C13a)}$$

$$y = \sin i \sqrt{(1-p)(1+q)/4}, \qquad \text{(C13b)}$$

that can be easily shown to coincide with the definitions in the bottom row of Table II.

The other cases reported in Table II (nearly equatorial or polar detector latitudes) can be derived analogously, the only difference being the shape of the integration domain in the (τ_d,η) rectangle. The above calculation can be specialized to annual averages during specific fractions of night, such as the period in which the Earth core is crossed [see Eq. (19) and related comments].

Concerning the case in which the time average is taken over a fraction of year (e.g., a season), we only mention that the weight function can still be expressed analytically, but the generic integration limits for τ_d require the calculation of the *incomplete* elliptic integral of the first kind (see [26] for its numerical evaluation). The possible cases for the functional form of $W(\eta)$ acquire an additional dependence on the fraction of year considered for the average, and are not discussed in this paper.

APPENDIX D: EFFECT OF EARTH-SUN DISTANCE VARIATIONS

Throughout this work, the Earth-Sun distance L has been taken constant ($L = L_0$), in the hypothesis that the trivial $1/L^2$ geometrical variations of the solar neutrino signal will be factorized out in real-time experiments. However, such a continuous correction of the data implies a real-time subtraction of the background and thus requires a difficult, daily task of monitoring background, efficiencies, and calibrations (which are instead better defined over long periods of time). Therefore, we consider also the effect of dropping the assumption of a real-time, geometric correction of the signal, for the relevant case of annual averages during (a fraction of) night time.

Given the orbital equation

$$L(\tau_d) = L_0[1 - \epsilon \cos(\tau_d - \tau_d^p)] + O(\epsilon^2), \qquad \text{(D1)}$$

where $\tau_d^p = 0.24$ corresponds to the perihelion and $\epsilon = 0.0167$ is the Earth orbit eccentricity, the time-averaged probability reads

$$\langle P_E \rangle'_{\text{night}} = \frac{\int_0^{2\pi} d\tau_d L^{-2}(\tau_d) \int_0^{\tau_h^{\text{sr}(\tau_d)}} d\tau_h P_E(\eta(\tau_d,\tau_h))}{\int_0^{2\pi} d\tau_d L_0^{-2} \int_0^{\tau_h^{\text{sr}(\tau_d)}} d\tau_h}. \qquad \text{(D2)}$$

We give without proof the final results for detector latitudes between the tropic and the polar circle (see also Table II):

$$\langle P_E \rangle'_{\text{night}} = \int_0^{\pi/2} d\eta W'(\eta) P_E(\eta), \qquad \text{(D3)}$$

$$W'(\eta) = W(\eta) \pm \epsilon Y(\eta), \qquad \text{(D4)}$$

where the upper (lower) sign refer to the northern (southern) hemisphere, $W(\eta)$ is given in Table II (first and third column), and the function $Y(\eta)$ is defined as

$$Y(\eta) = \frac{4}{\pi^2}\cos\tau_d^p\sin\eta \cdot \begin{cases} 0, & 0 \leq \eta < \lambda - i, \\ \frac{1}{z}\left[qK\left(\frac{y}{z}\right) - (q-1)\Pi\left(\frac{1-p}{q-p}, \frac{y}{z}\right)\right], & \lambda - i \leq \eta < \lambda + i, \\ \frac{1}{y}\left[qK\left(\frac{z}{y}\right) - (q-1)\Pi\left(\frac{2}{q+1}, \frac{z}{y}\right)\right], & \lambda + i < \eta \leq \pi/2. \end{cases} \tag{D5}$$

In Eq. (D5) the variables p, q, y, and z are defined as in Appendix C, and Π is the complete elliptic integral of the third kind [24,25],

$$\Pi(r,x) = \int_0^1 \frac{ds}{(1-rs^2)\sqrt{(1-s^2)(1-x^2s^2)}} \tag{D6}$$

(see [26] for its numerical evaluation).

The ''eccentricity correction'' $\pm\epsilon Y(\eta)$ is small. At latitudes of interest, the difference between annual averages with and without this term is less than 1%:

$$|\langle P_E\rangle'_{\text{night}} - \langle P_E\rangle_{\text{night}}| \leq \epsilon \int_0^{\pi/2} d\eta\, |Y(\eta)| = \begin{cases} 0.82\% & (\text{Kamioka}), \\ 0.95\% & (\text{Sudbury}), \\ 0.90\% & (\text{GranSasso}). \end{cases} \tag{D7}$$

Finally, we mention that, for averages over fractions of year, the eccentricity correction involves the evaluation of *incomplete* elliptic integrals of the third kind.

---

[1] L. Wolfenstein, Phys. Rev. D **17**, 2369 (1978); S. P. Mikheyev and A. Yu. Smirnov, Yad. Fiz. **42**, 1441 (1985) [Sov. J. Nucl. Phys. **42**, 913 (1985)]; Nuovo Cimento C **9**, 17 (1986).

[2] J. N. Bahcall, *Neutrino Astrophysics* (Cambridge University Press, Cambridge, England, 1989).

[3] S. P. Mikheyev and A. Yu. Smirnov, in *Moriond '86*, Proceedings of the 6th Moriond Workshop on Massive Neutrinos in Astrophysics and in Particle Physics, Tignes, France, 1986, edited by O. Fackler and J. Trân Thanh Vân (Frontières, Paris, 1986), p. 355.

[4] J. Bouchez, M. Cribier, W. Hampel, J. Rich, and D. Vignaud, Z. Phys. C **32**, 499 (1986); M. Cribier, W. Hampel, J. Rich, and D. Vignaud, Phys. Lett. B **182**, 89 (1986); A. J. Baltz and J. Weneser, Phys. Rev. D **35**, 528 (1987); **37**, 3364 (1988); A. Dar, A. Mann, Y. Melina, and D. Zajfman, *ibid.* **35**, 3607 (1987); A. Dar and A. Mann, Nature (London) **325**, 790 (1987); S. P. Mikheyev and A. Yu. Smirnov, in *Moriond '87*, Proceedings of the 7th Moriond Workshop on New and Exotic Phenomena, Les Arcs, France, 1987, edited by O. Fackler and J. Trân Thanh Vân (Frontières, Paris, 1987), p. 405; M. L. Cherry and K. Lande, Phys. Rev. D **36**, 3571 (1987); S. Hiroi, H. Sakuma, T. Yanagida, and M. Yoshimura, Phys. Lett. B **198**, 403 (1987); Prog. Theor. Phys. **78**, 1428 (1987); M. Spiro and D. Vignaud, Phys. Lett. B **242**, 279 (1990).

[5] T. K. Kuo and J. Pantaleone, Rev. Mod. Phys. **61**, 937 (1989).

[6] S. P. Mikheyev and A. Yu. Smirnov, Prog. Part. Nucl. Phys. **23**, 41 (1989).

[7] Kamiokande Collaboration, K. S. Hirata *et al.*, Phys. Rev. Lett. **66**, 9 (1991).

[8] Kamiokande Collaboration, Y. Fukuda *et al.*, Phys. Rev. Lett. **77**, 1683 (1996).

[9] N. Hata and P. Langacker, Phys. Rev. D **48**, 2937 (1993); **50**, 632 (1994).

[10] G. Fiorentini, M. Lissia, G. Mezzorani, M. Moretti, and D. Vignaud, Phys. Rev. D **49**, 6298 (1994).

[11] G. L. Fogli, E. Lisi, and D. Montanino, Phys. Rev. D **49**, 3626 (1994); Astropart. Phys. **4**, 177 (1995); Phys. Rev. D **54**, 2048 (1996).

[12] A. J. Baltz and J. Weneser, Phys. Rev. D **50**, 5971 (1994); **51**, 3960 (1995).

[13] P. I. Krastev, in *DPF '96*, Proceedings of the 1996 Annual Divisional Meeting of the Division of Particles and Fields of the American Physical Society, Minneapolis, MN, 1996 (to be published).

[14] Y. Totsuka, in *TAUP '95*, Proceedings of the 4th International Workshop on Theoretical and Phenomenological Aspects of Underground Physics, Toledo, Spain, edited by A. Morales, J. Morales, and J. A. Villar [Nucl. Phys. B, Proc. Suppl. **48**, 547 (1996)]; A. Suzuki, in *Physics and Astrophysics of Neutrinos*, edited by M. Fukugita and A. Suzuki (Springer-Verlag, Tokyo, 1994), p. 414.

[15] A. B. McDonald, Proceedings of the 9th Lake Louise Winter Institute, edited by A. Astbury *et al.* (World Scientific, Singapore, 1994), p. 1; *TAUP '95* [14], p. 357.

[16] E. Gates, L. M. Krauss, and M. White, Phys. Rev. D **51**, 2631 (1995).

[17] A. M. Dziewonski and D. L. Anderson, Phys. Earth Planet. Inter. **25**, 297 (1981).

[18] *Properties of the Solid Earth*, in Rev. Geophys. **33**, (1995); also available at the URL: http://earth.agu.org/revgeophys.

[19] A. M. Dziewonski and J. H. Woodhouse, Science **236**, 37 (1987).

[20] D. L. Anderson, Science **243**, 367 (1989).

[21] D. J. Stevenson, Science **214**, 214 (1981).

[22] F. Birch, J. Geophys. Res. **57**, 227 (1952), on p. 234: ''Unwary readers should take warning that ordinary language undergoes modification to a high pressure form when applied to the interior of the earth, e.g.,

High pressure form	Ordinary meaning
Certain	Dubious
Undoubtedly	Perhaps
Positive proof	Vague suggestion
Unanswerable argument	Trivial objection
Pure iron	Uncertain mixture of all the elements''

[23] J. N. Bahcall and M. H. Pinsonneault, Rev. Mod. Phys. **67**, 781 (1995).

[24] I. S. Gradshteyn and I. M. Ryzhik, *Tables of Integrals, Series, and Products* (Academic, San Diego, CA, 1994).

[25] M. Abramowitz and I. A. Stegun, *Handbook of Mathematical Functions with Formulas, Graphs, and Mathematical Tables* (Wiley, New York, 1972).

[26] CERN Program Library CERNLIB, subroutine packages C346 and C347 for the calculation of incomplete and complete elliptic integrals of the first, second, and third kind. A printable description of these routines can be found at the URL http://wwwcn.cern.ch/asdoc/cernlib.html.

[27] Borexino Collaboration, G. Bellini *et al.*, in *TAUP '95* [14], p. 363.

[28] ICARUS Collaboration, C. Rubbia *et al.*, in *TAUP '95* [14], p. 172.

[29] GNO Collaboration, ''Proposal for a permanent Gallium Neutrino Observatory (GNO) at Laboratori Nazionali del Gran Sasso'' (unpublished). The proposal is available at the URL http://kosmopc.mpi-hd.mpg.de/gallex/gallex.htm.

[30] HELLAZ Collaboration, T. Ypsilantis *et al.*, ''HELLAZ: a high rate solar neutrino detector with neutrino energy determination,'' College de France Report LPC/94-28 (unpublished).

[31] J. M. LoSecco, Phys. Rev. D **47**, 2032 (1993); J. M. Gelb, W. Kwong, and S. P. Rosen, Phys. Rev. Lett. **78**, 2296 (1997).

[32] P. J. Davis and P. Rabinowitz, *Methods of Numerical Integration* (Academic, San Diego, CA, 1984).

[33] J. N. Bahcall, E. Lisi, D. E. Alburger, L. DeBraeckeleer, S. J. Freedman, and J. Napolitano, Phys. Rev. C **54**, 411 (1996).

[34] J. N. Bahcall, Phys. Rev. D **44**, 1644 (1991).

[35] J. N. Bahcall, M. Kamionkowsky, and A. Sirlin, Phys. Rev. D **51**, 6146 (1995).

[36] J. N. Bahcall, P. I. Krastev, and E. Lisi, Phys. Rev. C **55**, 494 (1997); see also J. N. Bahcall and E. Lisi, Phys. Rev. D **54**, 5417 (1996).

[37] Tables of neutrino cross sections and moments of electron spectra, available at the URL http://www.sns.ias.edu/~jnb (see Neutrino Export Software and Data).

[38] SuperKamiokande Collaboration, K. Martens *et al.*, in the Proceedings of the 25th INS International Symposium on Nuclear and Particle Physics with High-Intensity Proton Accelerators, Tokyo, Japan, 1996 (to be published).

[39] D. Bruss and L. M. Sehgal, Phys. Lett. B **216**, 426 (1989).